

Soft Interactions and Diffractive Phenomena ¹

R. A. Eichler

Institute for Particle Physics, ETH-Zürich, CH 8093 Zurich

¹ Plenary talk PL2 at the Europhysics Conference on High Energy Physics, Jerusalem, August 1997

PL2: Soft Interactions and Diffractive Phenomena

Ralph Eichler (eichler@particle.phys.ethz.ch)

Institute for Particle Physics, ETH-Zürich, CH 8093 Zurich

Abstract. Recent results on hard diffraction at HERA and the Tevatron are presented. Charged particle multiplicities in diffraction and differences in multiplicity in quark and gluon jets measured at LEP are discussed. Spin effects in the fragmentation of leading quarks show some interesting features.

1 Total and Elastic Cross Section

The energy dependence on the center of mass energy \sqrt{s} of all hadron-hadron total cross sections is described by

$$\sigma_{tot}(s) = A_{IP}s^{\alpha_{IP}(0)-1} + A_{IR}s^{\alpha_{IR}(0)-1} .$$

with universal exponents $\alpha_{IP}(0)-1$ and $\alpha_{IR}(0)-1$ and process dependent constants A_{IP} and A_{IR} [1]. Regge theory, which relates poles in a t -channel scattering amplitude to energy behaviour in the s -channel gives a link to Regge trajectories $\alpha(t)$. The trajectories have been determined in hadron scattering and describe also surprisingly well $\gamma\gamma$ and γp scattering. The first term in the total cross section formula dominates the high energy behaviour and the corresponding Pomeron trajectory $\alpha_{IP}(t)$ is unique in Regge theory with largest intercept and vacuum quantum numbers: $\alpha_{IP}(t) = 1.08 + 0.25 \text{ GeV}^{-2} t$. Next leading reggeons have approximately degenerate trajectories and carry the quantum numbers of ρ, ω, a_2, f_2 mesons. They are combined in an effective trajectory $\alpha_{IR}(t) = 0.55 + 0.9 \text{ GeV}^{-2} t$.

Figure 1a shows a measurement by the L3 collaboration [2] of the total $\gamma\gamma$ cross section where the universal exponents have been assumed and coefficients $A_{IP} = 173 \pm 7 \text{ nb/GeV}^{-2}$ and $A_{IR} = 519 \pm 125 \text{ nb/GeV}^{-2}$ were fitted. Figure 1b presents the γp cross section as a function of the γp energy $W_{\gamma p}$ at photon virtualities $Q^2 \sim 0$. The elastic vector meson production $\gamma p \rightarrow V p$ with $V = \rho, \omega, \Phi, J/\Psi$ shows also a power law behaviour. The elastic cross section is related to the total cross section via the optical theorem

$$\left. \frac{d\sigma^{elastic}}{dt} \right|_{t=0}(\gamma p \rightarrow V p) \propto \sigma_{tot}^2 \propto (W^2)^{2(\alpha_{IP}(0)-1)} .$$

Figure 1b suggests that the growth $(W^2)^{2\lambda}$ is steeper for the heavier vector mesons, namely $\lambda = 0.22$ for J/Ψ -production [3] compared to the value for σ_{tot} , namely $\lambda = \alpha_{IP}(0) - 1 = 0.08$. For elastic ρ -production the exponent

λ grows from 0.08 at low Q^2 to 0.19 ± 0.07 at $Q^2 = 20 \text{ GeV}^2$ [4]. Apparently λ is a function of the hardness of the scale (quark mass, Q^2) involved in the scattering.

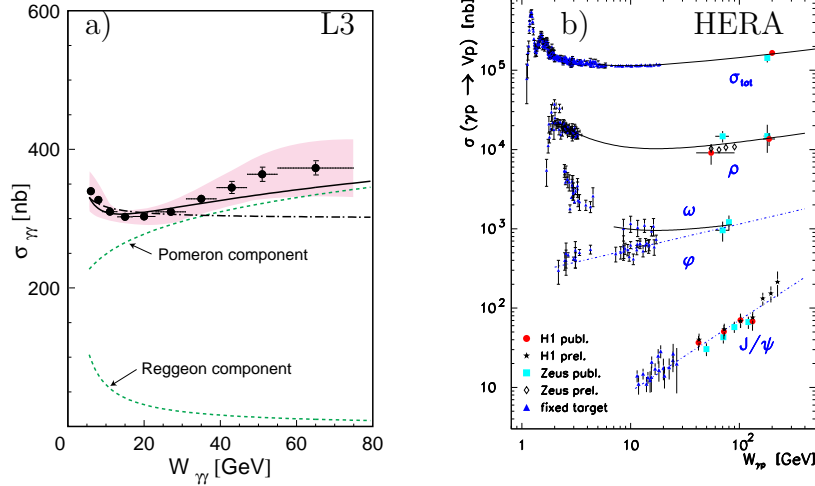


Fig. 1. a) total $\gamma\gamma$ cross section versus $\gamma\gamma$ energy $W_{\gamma\gamma}$. The shaded band is the systematic error, solid line a fit of the sum of Pomeron and Reggeon component. b) quasireal total and exclusive vector meson γp cross section with photon virtuality $Q^2 \sim 0$ vs γp center of mass energy $W_{\gamma p}$. The lines are a fit to the data.

2 Inelastic Diffraction

Diffraction scattering has been observed in $h-h$ interactions a long time ago. A typical signature is a forward peaked beam particle which remains intact or is excited to a small mass M_Y and a rapidity gap between it and the rest of the final state X (Figure 2a).

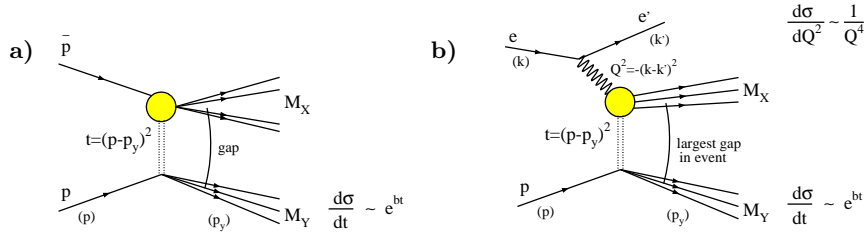


Fig. 2. a) Diffractive scattering in $p\bar{p}$ interactions. Hard diffraction is observed in reactions, where the system X consists of jets. b) diffractive scattering in deep inelastic ep interactions. Without detection of the leading proton experimental cuts constrain $t < 1 \text{ GeV}^2$ and the mass $M_Y < 1.6 \text{ GeV}$ (H1), $< 4 \text{ GeV}$ (ZEUS).

Diffractive scattering has also been observed in deep inelastic scattering (DIS) at HERA with a fraction of roughly 10% of total DIS. The kinematics is

defined through the measurement of the scattered positron, the mass M_X of the system X via the hadronic final state and the observation of a gap between X and Y , fig. 2b. The standard DIS variables are $q = k - k'$, $Q^2 = -q^2$, $W^2 = (p + q)^2$, $x_{Bj} = q^2/2P \cdot q$ and the additionally measurable variables

$$x_{IP} \equiv \xi = \frac{M_X^2 + Q^2 - t}{W^2 + Q^2 - m_p^2}, \quad \beta = \frac{Q^2}{2q \cdot (p - p_Y)} = \frac{x_{Bj}}{\xi} = \frac{Q^2}{M_X^2 + Q^2}.$$

The variable $t = (p - p_Y)^2$ is known only if the scattered proton is detected in the leading proton spectrometer, otherwise data from the forward detectors only limit t and M_Y (see caption of figure 2). The intuitive meaning of $\xi = x_{IP}$ and β can be best understood in the infinite momentum frame of the proton. Consider the Feynman diagrams of Figure 3. The virtual photon γ^* probes partons in the diffractively exchanged object which carries a momentum fraction x_{IP} of the proton. These partons carry a fraction β of this object [5]. In the following it will be shown, that this diffractively exchanged object can be viewed as in the formula of σ_{tot} as a sum of a Pomeron and a Reggeon term.

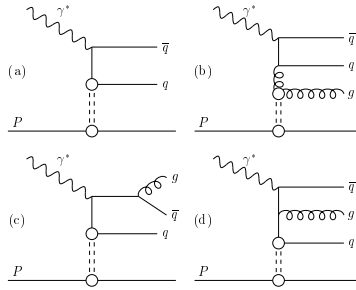


Fig. 3. Lowest order Feynman diagrams of inelastic diffraction in DIS. The dotted double line indicates the diffractively exchanged object in the infinite momentum frame of the proton.

An equivalent picture of diffraction is seen in the proton rest frame [6, 7, 8, 9, 10]. The Fock states of the photon $|\gamma\rangle = |q\bar{q}\rangle, |q\bar{q}g\rangle, \dots$ etc are formed long before the target (Ioffe length $\ell \sim 1/x \sim$ several 100 fm) and the quark pairs interact softly through multiple gluon exchange with the target. Despite hard scattering at large Q^2 the target is only hit gently. The rapidity gap formation is then a long time scale process after the quark pair has traversed the proton and the diffractively produced final states X are expected to be sensitive to the topology and colour structure of the partonic fluctuations of the virtual photon.

2.1 Results from Leading Proton Spectrometer at HERA

Figure 4 shows preliminary results from the ZEUS leading proton spectrometer [11]. The device measures the energy E'_p of the scattered pro-

ton and its transverse momentum p_t . The kinematical variables are defined $x_L = 1 - \xi = E'_p/E_p$ and $t = -p_t^2/x_L - m_p^2(1 - x_L)^2/x_L$. A clear diffractive peak at $x_L = 1 - \xi > 0.97$ is observed and the b -parameter ($d\sigma/dt \propto e^{bt}$) was fitted and found to be between 4 and 10 depending on x_L [11].

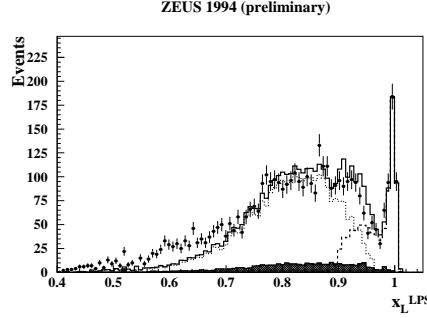


Fig. 4. Preliminary results from the ZEUS leading proton spectrometer.

2.2 Diffractive Structure Function

The fivefold differential cross section defines the diffractive structure function $F_2^{D(5)}$ with five variables [12]

$$\frac{d^5\sigma_{ep \rightarrow eXY}}{d\beta dQ^2 d\xi dt dM_Y} = \frac{4\pi\alpha^2}{\beta Q^4} (1 + (1 - y)^2) F_2^{D(5)}(\beta, \xi, Q^2, t, M_Y).$$

To gain statistics the final state proton is not detected and the variables M_Y and t are not measured. Therefore one defines a new structure function by integrating over the variables t and M_Y . (H1: $|t| < 1 \text{ GeV}^2$ and $M_Y < 1.6 \text{ GeV}$, ZEUS: $|t| < 1 \text{ GeV}^2$ and $M_Y < 4.0 \text{ GeV}$)

$$\frac{d^3\sigma_{ep \rightarrow eXY}}{d\beta dQ^2 d\xi} = \frac{4\pi\alpha^2}{\beta Q^4} (1 + (1 - y)^2) F_2^{D(3)}(\beta, \xi, Q^2).$$

H1 made an Ansatz for $F_2^{D(3)}$ as a sum of Pomeron exchange and Reggeon (Meson) exchange [13]. Each term factorises into a Pomeron/Meson flux dependent function of ξ, t and a structure function dependent on β, Q^2 :

$$F_2^{D(3)}(\beta, \xi, Q^2) = \int dt \left[\frac{e^{B_{IP}t}}{\xi^{\alpha_{IP}(t)-1}} F_2^{IP}(\beta, Q^2, t) + C_M \frac{e^{B_{IR}t}}{\xi^{2\alpha_{IR}(t)-1}} F_2^M(\beta, Q^2, t) \right]$$

plus a possible interference term (since the f_2 -meson and the IP have the same C-parity). In the above expression the integral is over $|t| < 1 \text{ GeV}^2$.

The measurements of H1 were fitted in 47 bins in $4.5 \text{ GeV}^2 \leq Q^2 \leq 75 \text{ GeV}^2$, $0.04 \leq \beta \leq 0.9$ with free parameters $\alpha_{IP}(0), \alpha_{IR}(0), C_M$. A very good fit confirms the Ansatz and two such examples are shown in Figure 5.

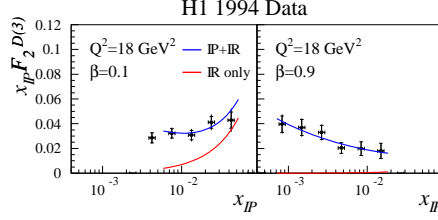


Fig. 5. $x_{IP} F_2^{D(3)}(\beta, Q^2)$ as a function of x_{IP} for two bins in Q^2 and β .

Contributions of the meson term is noticeable at $\xi = x_{IP} > 0.01$ and small β (large M_X). As a result H1 gets [13]

$$\alpha_{IP}(0) = 1.203 \pm 0.02(stat) \pm 0.013(syst)_{-0.035}^{+0.03}(model)$$

$$\alpha_{IR}(0) = 0.50 \pm 0.11(stat) \pm 0.11(syst) \pm 0.10(model).$$

An analysis of the ZEUS collaboration [14] with a fit at fixed Q^2

$$\frac{d\sigma_{ep \rightarrow eXY}^D}{dM_X} \sim (W^2)^{2\alpha_{IP}-2}$$

where the non-diffractive background has been parametrised and subtracted first yields a similar result for $\alpha_{IP}(0)$ (see Figure 6).

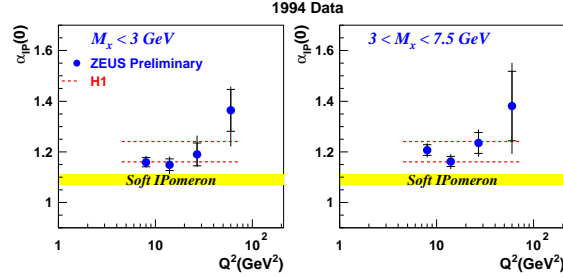


Fig. 6. $\alpha_{IP}(0)$ vs Q^2 in two bins of M_X . The band limited by the dotted lines indicate the range in $\alpha_{IP}(0)$ from the H1 analysis. The shaded band is the value found in soft processes like σ_{tot} .

The results of the two experiments are consistent with each other and the intercept in hard diffraction is larger than $\alpha_{IP}(0) = 1.08$ determined from σ_{tot} .

The diffractive structure function shows scaling violation as depicted in Figure 7. The structure function rises with Q^2 up to very high $\beta = 0.65$ values [13, 16]. The H1-Ansatz for $F_2^{D(3)}$ has been taken and the two structure functions F_2^{IP} and F_2^M parametrised at a fixed $Q_0^2 = 3GeV^2$ through parton

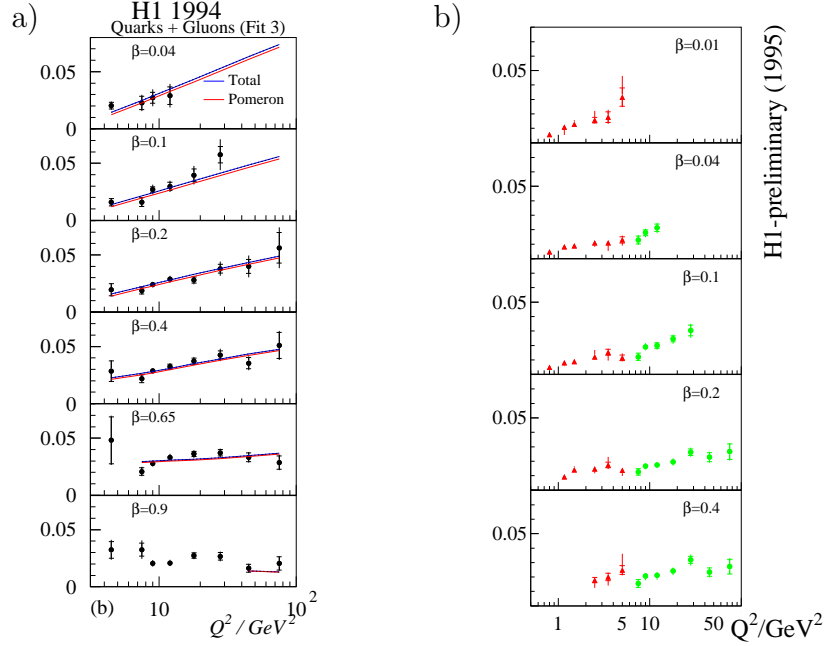


Fig. 7. Scaling violation of the diffractive structure function $\xi F_2^D(\xi, \beta, Q^2)$ at fixed $\xi = 0.003$ (a) and $\xi = 0.005$ (b) vs Q^2 . The solid line is a DGLAP fit.

distributions. These parton distributions are evolved according to Dokshitzer-Gribov-Lipatov-Altarelli-Parisi (DGLAP) [15] equation to any other Q^2 and compared with the data. For the meson piece, F_2^M , a pion structure function was taken. For the Pomeron piece the ratio of quarks and gluons at the starting scale Q_0^2 and its corresponding shapes were fitted with the result that 90% of the Pomeron momentum is carried by gluons at $Q^2 = 4.5 \text{ GeV}^2$ and still 80% at $Q^2 = 75 \text{ GeV}^2$.

2.3 Hard Diffraction at the Tevatron

Hard diffraction has also been observed in $p\bar{p}$ collisions at the Tevatron where the hardness scale is given by the required jets in the final state or the production of a heavy gauge boson like W . Three processes are considered:

1. $p + \bar{p} \rightarrow p + \text{gap} + (X \rightarrow \text{jet1} + \text{jet2} + X')$. The kinematics has been defined in Figure 2a. Without the measurement of the final state proton the kinematical variable ξ cannot be measured. Its distribution is taken from MC model calculations (POMPYYT) with a factorised Pomeron flux $f_{IP/p}(\xi, t) = \frac{K}{\xi^{2\alpha_{IP}(t)-1}} F^2(t)$ and a hard Pomeron structure function $\beta G(\beta) = 6\beta(1 - \beta)$ [5]. In this model ξ is restricted through the final state topology to $0.005 \leq$

$\xi \leq 0.015$. The ratio of diffractive dijets to all dijets with $E_T > 20\text{GeV}$ is $R_{JJ} = 0.75 \pm 0.05(\text{stat}) \pm 0.09(\text{syst})\%$ (CDF [17]), and $0.67 \pm 0.05(\text{stat})\%$ (D0). This ratio is sensitive to the relative ratio of quarks and gluons in the Pomeron.

2. $p + \bar{p} \rightarrow p + (W \rightarrow e\nu + X')$. The gluon content in the Pomeron does not contribute much (suppressed by α_s). The result from CDF [18] for the ratio of diffractive to non-diffractive W-production $R_W = 1.15 \pm 0.55(\text{stat}) \pm 0.20(\text{syst})\%$.

3. $p + \bar{p} \rightarrow jet1 + gap + jet2$. Rapidity gaps of size $\Delta\eta$ between jets from fluctuations in fragmentation are exponentially suppressed. Figure 8 shows data from D0 [19] where the fraction of events with a large gap as a function of the jet E_T (fig. 8a) and as a function of $\Delta\eta$ (fig. 8b) are plotted.

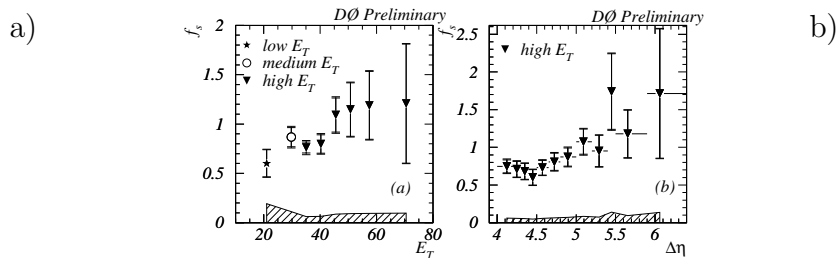


Fig. 8. Fraction f_s [%] of events with a rapidity gap between jets vs jet E_T (a) and vs the gap size $\Delta\eta$ (b).

It has become clear during the year, that not all 3 types of observations can be explained by this simple factorised POMPYT model. It remains to be seen if factorisation could be restored as in the case of HERA.

3 Fragmentation

3.1 Charged Multiplicity in Diffraction at HERA

Fragmentation gives the link between cross section on the parton level and observed particles in the detector. The charged particle multiplicity grows with the CM energy, with \sqrt{s} in e^+e^- annihilation and with W in lepton-proton scattering. It has been shown that the multiplicity is independent of Q^2 [20]. The question arises if the diffractive system X defined in Figure 2b fragment as an independent object, i.e. is the multiplicity in diffraction governed by M_X or still by W ?

In Figure 9 we compare the particle density $\frac{1}{N} \frac{dn}{dy}$ at the plateau [21] as a function of M_X and compare it to inclusive (non-diff) DIS at $W = M_X$. The multiplicity in diffractive events is about 0.6 units higher. We conclude that hadronisation in diffraction cannot be described by the fragmentation

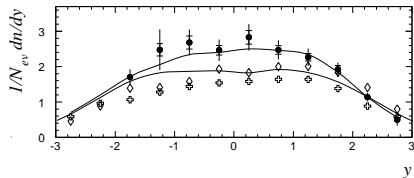


Fig. 9. Particle density $1/N dn/dy$ as a function of rapidity for $M_X = 22.5 \text{ GeV}$ (full symbols, H1), for $W = 19 \text{ GeV}$ (open crosses, EMC μp) and for $W = 23.4 \text{ GeV}$ (open circle, E665 μD). The full curve is the RAPGAP simulation for γp processes and the dashed line from JETSET (e^+e^-).

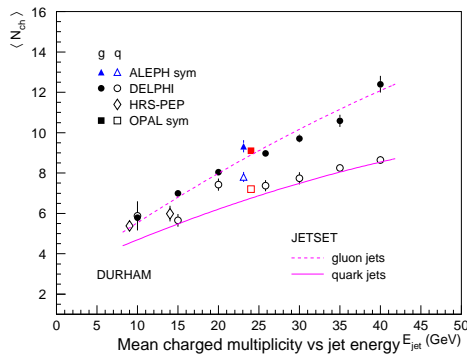


Fig. 10. Mean charged multiplicity vs jet energy for gluon jets (full symbols) and quark jets (open symbols).

of a single colour string as implemented in the Lund model. The dominant diagram according to [7] is the one in Figure 3c where the system X is rather a colour octet string.

3.2 Charged Multiplicities in Quark and Gluon Jets

One expects a larger multiplicity in gluon jets than in quark jets because of the stronger effective $g \rightarrow gg$ than $q \rightarrow qq$ coupling. Gluon initiated jets are selected at LEP in a 3-jet $q\bar{q}g$ topology, where the jets with identified heavy quarks are taken as quark initiated jets. The effect of a larger multiplicity of the remaining gluon jets (75-90% purity) is clearly seen in Figure 10 where results from all four LEP experiments are shown [23].

3.3 Leading Particles in Fragmentation

Leading particles carry quantum numbers such as flavour and spin of the primary produced partons. This is demonstrated for flavours in a result of SLD (Figure 11) and for spin in LEP results.

The polarised initial state in $e^+e^- \rightarrow q\bar{q}$ at SLC allows the distinction of a quark initiated jet as opposed to an antiquark jet. Consider jets from light flavours u, d, s and let $N(q \rightarrow h)$ be the number of hadrons of type h from quark jets. The production rate R and the difference D are defined

$$R_h^q = \frac{1}{2N_{evts}} \frac{d}{dx_p} [N(q \rightarrow h) + N(\bar{q} \rightarrow \bar{h})], \quad D_h = \frac{R_h^q - R_{\bar{h}}^q}{R_h^q + R_{\bar{h}}^q}.$$

Figure 11 plots D_h vs x_p [25]. One sees clear evidence for production of leading baryons at high x_p . Also K^- and \bar{K}^* are dominant over their antiparticles at high x_p .

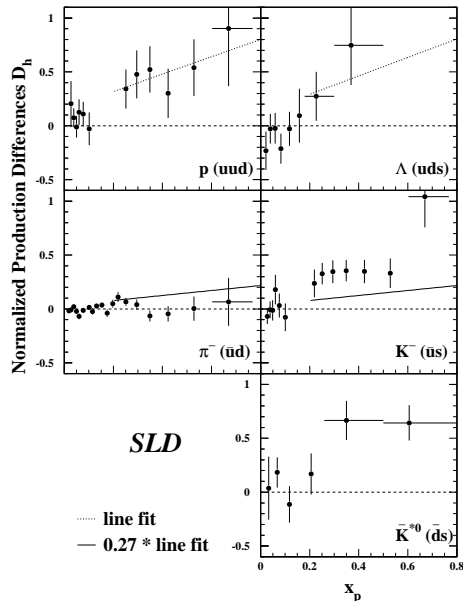


Fig. 11. Normalized production differences D_h between particles in quark jets and particles in antiquark jets vs x_p . The dotted lines represent the results of a linear fit to the baryon data for $x_p > 0.2$, and the solid lines represent this fit scaled by a dilution factor 0.27 valid for pions.

Quarks from $Z^0 \rightarrow q\bar{q}$ are polarised. It has been known since several years, that this polarisation is transferred to the first rank baryons $\Lambda, \Lambda_c, \Lambda_B$. LEP measured a Λ -polarisation of $p_\Lambda = -32.9 \pm 7.6\%$ (OPAL [22]) and $-32 \pm 7\%$ (ALEPH). This is explained if the s-quark carries the spin of the Λ particle.

In $J^P = 1^-$ vector mesons any spin alignment must arise from hadronisation. The spin density matrix ρ_{ij} can be measured through angular dependence of the decay mesons with respect to the spin quantisation axis $W(\cos\theta_H) = \frac{3}{4} [(1 - \rho_{00}) + (3\rho_{00} - 1)\cos^2\theta_H]$.

In a statistical model [24] $\rho_{00} = \frac{1}{2}(1 - P/V)$ with P/V ratio of pseudoscalar to vector mesons in fragmentation. In this model $\rho_{00} \leq 0.5$ and $\rho_{00} = 0$ for $P/V = 1$, $\rho_{00} = 1/3$ for $P/V = 1/3$.

Results from CLEO, HRS, TPC-2 γ , ALEPH, DELPHI, OPAL give $\rho_{00} \sim 1/3$ for ρ, D^*, B^* -mesons, $\rho_{00} > 1/3$ for D^*, Φ, K^* -mesons at large fractional momentum, and even $\rho_{00} = 0.66 \pm 0.11$ for K^* at $x_p > 0.7$ [26]. A value of $\rho_{00} > 0.5$ is an interesting observation and is not explained in any fragmentation model.

4 Summary

Multi-dimensional distributions in diffraction at the Tevatron and the precision data of HERA help the understanding of diffractive phenomena. The semi-inclusive cross sections rise with energy proportional $(W^2)^\lambda$ where λ

grows with the hard scale involved. Inelastic diffraction using only Pomeron exchange breaks factorisation, both at HERA and the Tevatron. A sum of Pomeron exchange (80% gluons) and meson exchange (quark-dominated exchange) restores factorisation at HERA. The particle density dn/dy at fixed M_X is larger in diffractive DIS than in non-diffractive DIS at the corresponding $W_{\gamma p}$ which is related to a more complex colour string in diffraction than in non-diffractive DIS. Fragmentation properties of gluon jets are well measured at LEP and show a larger charged multiplicity in gluon initiated jets than in quark jets. Large spin alignment of leading vector mesons at Z^0 is observed, which is an interesting observation and not explained so far.

References

- [1] A. Donnachie and P.V. Landshoff, Phys.Lett.B296(1992)227
- [2] L3-Collaboration, M. Acciarri et al., Phys. Lett. B408 (1997) 450
- [3] H1-Collaboration, S. Aid et al., Nucl.Phys. B472(1996)3
- [4] ZEUS-Collaboration, contributed paper#639 this conference
- [5] G. Ingelmann and P.E. Schlein, Phys.Lett. B152(1985)256
- [6] J.D. Bjorken and J. Kogut, Phys.Rev. D8 (1973) 1341
- [7] W. Buchmüller and A. Hebecker, Phys.Lett. B355(1995)573; A.Edin, G. Ingelmann and J. Rathsmann, Phys.Lett. B366(1996)371; W. Buchmüller, M.F. McDermott and A. Hebecker, hep-ph/9607290
- [8] S. Brodsky, P. Hoyer and L. Magnea, Phys.Rev. D55(1997)5585
- [9] N.N. Nikolaev and B.G. Zakharov, Z.Phys. C49(1991) 607; Z.Phys.C64(1994)631
- [10] D.E. Soper, hep-ph/9707384
- [11] ZEUS-Collaboration, contributed paper#644 this conference
- [12] A. Berera and D.E. Soper, Phys.Rev. D50(1994) 4328; Phys.Rev. D53(1996) 6162; G. Veneziano, L. Trentadue Phys.Lett. B323(1994)201
- [13] H1-Collaboration, C. Adloff et al., DESY 97-158
- [14] Zeus-Collaboration, contributed paper#638 this conference
- [15] Yu.L. Dokshitzer, Sov.Phys. JETP 46 (1977) 641; V.N. Gribov and L.N. Lipatov, Sov. J. Nucl. Phys. 15 (1972) 438,675; G. Altarelli and G. Parisi, Nucl.Phys. B126 (1977) 298
- [16] H1-Collaboration, contributed paper#377 this conference
- [17] CDF-Collaboration, contributed paper LP97, Hamburg (1997)
- [18] CDF-Collaboration, F. Abe et al., Phys.Rev.Lett. 78(1997)2698
- [19] D0-Collaboration, contributed paper#800 this conference
- [20] H1-Collaboration, C. Adloff et al., Z.Phys. C72(1996)573
- [21] H1-Collaboration, contributed paper#250 this conference
- [22] Opal-Collaboration, K. Ackerstaff et al., CERN-PPE/97-104
- [23] LEP experiments, see contributed paper #683 this conference
- [24] J.F. Donoghue, Phys.Rev. D19(1979)2806
- [25] SLD-Collaboration, contributed paper#287 this conference
- [26] OPAL-Collaboration, K. Ackerstaff et al., CERN-PPE/97-094,